PULSATILE MHD FLOW OF TWO IMMISCIBLE NANOFLUIDS THROUGH A POROUS CHANNEL WITH SLIP EFFECTS

Padma Devi Medisetty[*], Srinivas Suripeddi, and Satyanarayana Badeti
Department of Mathematics, VIT-AP University, Inavolu, Amaravathi-522237, Andhra Pradesh, INDIA
E-mail: padmadevimedisetti@gmail

Vajravelu Kuppalapalle
University of Central Florida, FL32816, Orlando, USA

The present study investigates the effects of shape factor nanoparticles on an oscillatory MHD flow of a nanofluid in two immiscible liquids in a horizontal porous channel with velocity and thermal slip on the walls. Thermal radiation, Joule heating, viscous and Darcy dissipations have been accounted for in the model. We have considered Al_2O_3 and Cu as nanoparticles, in the lower region (Region-I) and upper region (Region-II): respectively, with water as a base fluid. The effective ratio of thermal conductivity of the nanofluid is evaluated using the Maxwell-Garnetts model. The behavior of velocity, temperature, and rate of heat transfer distributions have been depicted graphically for the cases of slip and no-slip effects. This study has been made to understand the impact of different nanoparticle shape factors on temperature and the heat transfer rate. For various parameters, values of shear stress distribution at the walls and the mass flux are shown in a tabular form. Our study asserts that with the increase of the strength of the magnetic field, the velocity of the liquid falls and enhances the temperature of the liquid. The influence of different combinations of nanoparticles on the flow variables have also been discussed. In order to validate the analytical results, the numerical evaluation of the closed-form results for the velocity distribution has been compared with those of the numerical method, by using the NDSolve command in MATHEMATICA, and a good agreement is observed.

Key words: velocity and thermal slips, Darcy dissipation, Joule heating, volume fraction, shape factor.

1. Introduction

Several scientific and technical areas involve research concerning multiphase flow, heat transfer, and multicomponent mass transport in a porous space. Important technological applications include thermally enhanced oil recovery, subsurface contamination and remediation, high-level radioactive waste dumps, thermal insulating materials, multiphase trickling bed reactors, nuclear reactor safety analyses, drying procedures, and geothermal energy. These are just a few of the many engineering applications (Wang and Cheng [1] and several references therein). Two immiscible flows have been widely used in industrial equipment such as cooling systems, heat exchangers, nuclear reactors, and so on. As a result, it is critical to explore the multi-fluid flow condition, particularly the interaction between different types of fluids. An extensive survey of the literature reveals that two immiscible fluids in the same geometry have attracted significant attention so far. Packham and Shall [2] studied the stratified laminar flow of two immiscible liquids in a horizontal pipe.

Enhancement of heat transfer has resulted in an extensive use of pulsating flow. Liquid flows with periodic variations, in geometries of different cross-section is an important subject of study. It is important in industrial and biological processes such as the respiratory and circulatory systems, reciprocating pumps, vascular diseases, IC engines, pulse combustors, and blood dialysis in artificial kidneys. There are many practical applications in engineering and biomechanical systems like transpiration cooling, gaseous diffusion,

---

[*] To whom correspondence should be addressed

pulsated heat exchangers, reciprocating engines, barge-mounted floating nuclear reactors, and many others. For applications in manufacturing, thermal engineering, electronic engineering, chemical engineering, medicine, and biology, pulsating flows improved heat transfer characteristics [3-7]. It is recognized and confirmed by Mladin and Zumbrunnen [8] that fluid pulsation enhances heat transfer because of its properties, such as instability processes, turbulence, asymmetrical mixing, and nonlinear dynamic change on the thermal boundary layer. Using the perturbation method, Radhakrishnamacharya and Maiti [9] examined the characteristics of heat transfer in a permeable channel with a periodic pressure gradient. Kumar and Suripeddi [11] analysed numerically a hydromagnetic pulsating flow of the Eyring-Powell nanofluid with blood as the base fluid and alumina (Al_2O_3): copper (Cu): silver (Ag): and gold (Au) as nanoparticles in a vertical porous channel with the effects of Joule's heating, viscous dissipation and thermal radiation. The constitutive relation for the heat flux vector was studied by Ezzat and E.L. Bray [12]. Therefore, studies to improve the efficiency of heat transfer pulsating flows have attracted more attention in recent years.

Nanoliquids developed by suspension of nanosized particles (*10-50nm*) or fibers in a liquid have a significant potential for enhancing heat transfer in liquids because nanoliquids have anomalously increased thermal conductivity nature [13, 14]. One method for increasing the heat transfer rate is to increase the fluid's conducting properties. This enhancement is possible through the use of nanofluids, which are a combination of a base fluid (often water, oil, or ethylene glycol) and high thermal conductivity metallic nanoparticles such as Cu, Al_2O_3, SiO_2, and others. Nanofluid technology has recently been applied in a variety of technological applications that include refrigeration, cooling applications, thermal management, thermal energy storage, and convective heat transfer control. Recent studies on nanofluids have revealed that the flow conditions change when nanoparticles are added because their thermal conductivity is substantially higher than that of basic fluids. Nanofluids have a wide range of applications in the electrical, engineering, and medicinal fields. Nanofluids are frequently used in industrial heating and cooling systems, hyperthermia, electronic device batteries, and contemporary medicine delivery techniques. Eastman *et al.* [15] reported that *5%* nanoparticle volume fractions of Al_2O_3-water and CuO-water enhanced the thermal conductivity by *29%* and *60%* percent, respectively Xie *et al.* [16] reported that Al_2O_3 ethylene glycol with a *5%* nanoparticle volume fraction increased thermal conductivity by *30%*. The problem of natural convection past a vertical plate, proposed by the Cheng-Minkowycz, in a porous space saturated by a nanoliquid is studied analytically by Nield and Kuznetsov [17]. Philip and Shima [18] published a general overview of current developments in the field of nanofluids, focusing on key material characteristics that have a significant impact on the thermal properties of nanofluids and cutting-edge methods to attain incredibly high thermal conductivities. The thermal characteristics of a two-dimensional boundary layer flow over a moving surface immersed in a nanoliquid are reported by Bachok *et al.* [19]. Kasaeian *et al.* [20] presented a most recent research on nanofluids flow in various geometries. In water and toluene environments, the thermal conductivities of two different types of Au nanoparticles were measured.

The study of porous media transport phenomena has received significant attention due to its importance in industrial and technical applications. Fluid flow and heat transmission in porous media have attracted a lot of attention in recent decades. This is primarily due to the numerous applications of flow through a porous medium, such as radioactive nuclear waste storage, transpiration cooling, separation processes in chemical industries, filtration, aquifer transport processes, groundwater pollution, geothermal extraction, and fiber insulation. Drying technology, thermal insulation, catalytic processes, crowded bed heat exchangers, geothermal systems, petroleum industries, and electronics cooling are some of applications (Khanafer and Vafai [21]). Porous media are also used in biomedical applications, such as the delivery of drugs, the creation of porous tissue-engineering frames, and the manufacture of tissues for tissue replacement. Vafai and Tien [22] utilize the Darcy law to explain the exact connection between the Darcian velocity and the pressure drop throughout porous media. Khaled and Vafai [23] examined the diversity of biomedical zones including blood flow in tumors by using porous media models, brain tissue diffusion, and bio-heat transmission in tissues. The study pertaining to porous space and nanoliquid has gained considerable attention in recent times, and led to several explorations in this domain. The contact surface area between the solid surface and the liquid is increased by porous media, and due to the presence of dispersed nanoparticles in the nanofluid, the effective thermal conductivity will be raised. It appears that utilizing both the porous medium and nanoliquid can

significantly increase the convectional thermal systems efficiency. The steady, fully developed mixed convection nanofluid flow in an inclined channel filled with a porous medium was studied by Cimpean and Pop [24]. Natural convection in a partially porous cavity filled with a nanofluid was investigated by Chamkha and Ismael [25]. The effects of variable surface heat flux and first-order chemical reaction on an MHD flow and radiation heat transfer of nanofluids against a flat plate in porous media was examined by Zhang *et al.* [26]. Vijayalakshmi and Srinivas [27] studied the hydromagnetic pulsating nanofluid flow in a porous channel with thermal radiation. Umavathi and Hemavathi [28] studied the heat transfer of a clear, viscous fluid-filled vertical channel sandwiched between a porous medium-saturated nanofluid. Nazeer *et al.* [29] investigated the steady flow of a third-grade fluid due to a pressure gradient between two parallel plane walls that are maintained at different temperatures. It is presumed that the region between the plane's walls is a porous space having a constant permeability. Ezzat et.al.[30] applied the state space approach and the inversion of the Laplace transformation method to solve the non-dimensional equations of an unsteady laminar free convection flow of an incompressible, viscous, electrically conducting dusty fluid through a porous medium.

The majority of research on nanofluid flows focuses on a boundary layer flow and heat transfer in incompressible Newtonian fluids. Ohmic dissipation can also be generated by using the magnetic effect in Newtonian fluid flows. This effect, which is also called Joule thermoelectric heating, can be used in many devices with direct current. These include silicate glass melt synthesis with electrode-dependent Joule dissipation, electrochemical machining with electrolytic solutions, and magnetically responsive composite materials manufacture. The Joule heating consideration in energy expression describes the thermal gradient and changes in temperature. This phenomenon has applications in geophysical streams and nuclear engineering. Viscous dissipation changes the temperature distributions by acting like a source of energy, which affects the rate of heat transfer. Heat transport analysis over porous surfaces is of great practical importance. Daniel *et al.* [31] studied the combined effects of thermal radiation and viscous dissipation in a two-dimensional steady flow of electrically conducting nanofluid, using Buongiorno's model. The effects of viscous dissipation, thermal radiation, and Ohmic heating on the magnetohydrodynamic pulsatile flow of a third-grade hybrid nanofluid in a porous space was examined by Govindarajulu and Subramanyam Reddy [32]. Wahid *et al.* [33] studied the magnetohydrodynamic (MHD) stagnation point flow of an alumina-water nanofluid caused by a contracting sheet while taking into account the effects of viscous dissipation, melting, and Joule heating.

One important factor that impacts the nanoliquids flow is the magnetohydrodynamic (MHD) effect. Alfven was the first to introduce the term magnetohydrodynamic (MHD). Based on the magnetohydrodynamics hypothesis, a magnetic field induces a current in a moving conductive fluid, which applies a force on the ions of the conductive fluid. The two-dimensional magnetohydrodynamic (MHD) flow analysis with thermal radiation in a channel with porous walls was made by Hayat *et al.* [34]. Hatami *et al.* [35] investigated the MHD nanofluid in forced-convection boundary layer, assuming base fluid as water and aluminaoxide as a nanoparticle, over a horizontal plate. Sheikholeslami *et al.* [36] studied the magnetohydrodynamics nanofluid flow between two horizontal rotating plates, accounting for the thermal radiation effect. Sandeep and Reddy [37] studied the electrically conducting magnetohydrodynamic nanofluid flow's capacity to transfer heat over a cone and a wedge. They considered nonlinear thermal radiation, viscous dissipation, Joule heating, and non-uniform heat source/sink effects. The combined heat and mass transfer of a perfect conducting micropolar fluid near an infinite vertical surface in MHD natural convection is investigated by Ezzat *et al.* [38]. Furthermore, various theoretical and numerical studies have shown that a slip velocity exists between solid-fluid interfaces. Raisi *et al.* [39] examined the impact of slip and no-slip boundary conditions on the flow field and heat transfer while analyzing the thermal performance of a microchannel cooled with either pure water or a *Cu*-water nanofluid. Bitla and Iyengar [40] investigated the motion of a micropolar liquid, with a periodic pressure gradient, through a channel surrounded by permeable beds with slip boundary conditions. Adesanya and Makinde [41] investigated the effect of slip on the hydromagnetic pulsatile flow through a channel with a saturated porous medium and time-dependent boundary conditions on the heated wall. An analytical analysis was conducted by Srinivas *et al.* [42] to examine the effects of chemical reactions on the MHD nano liquid flow with heat source/sink in a contracting/expanding porous pipe. In the presence of thermal radiation, the properties of the heat transfer flow of a nanoliquid in a porous space with varying permeabilities were examined by Vijayalakshmi and Srinivas [43]. The influence of velocity slip on the peristaltic MHD flow of a nanofluid in

a porous-spaced non-uniform channel with Joule heating was examined by Sucharitha *et al.* [44]. Goodarzi *et al.* [45] investigated the effect of using aluminum oxide nanoparticles in a non-Newtonian fluid of aqueous solution of carboxymethyl cellulose in microtubes and by applying different slip coefficients to obtain different qualities on microtube surfaces.

The properties of nanoparticles, which are different from those of the corresponding bulk materials determine the particle size [13, 46, 47]. To explain the size-dependent properties, several models [46, 48], have been applied, where the nanoparticles are considered as ideal spheres. Chamkha *et al.* [49] studied the control-volume-based finite element method to numerically examine the enclosure of natural convection of a magnetohydrodynamic nanofluid under the influences of radiation of heat and the form factor of nanoparticles (CVFEM). Examples of the shapes of nanoparticles employed in the study include columns, spheres, and lamina. Sobamowo [50] analyzed the free convection flow of different nanofluids with shape factors, over a vertical plate for small and large Prandtl values. Shah *et al.* [51] studied the migration of nanomaterials through a permeable domain that was modeled numerically. They considered aluminium oxide as a testing fluid and water as the base fluid. Dogonchi *et al.* [52] studied an inclined elliptical heater with natural convection in a cavity under the influence of a magnetic field, with different shape factors of nanoparticles, using the CVFEM approach. Various methods of preparation of nanoparticles have been developed (Cele [53]) and they are suitable for synthesis of nanoparticles in different sizes and shapes. Hazarika *et al.* [54] investigated the hydromagnetic flow of a water-based nanofluid including copper (*Cu*): silver (*Ag*): and ferrous ferric oxide (*Fe$_3$O$_4$*) nanoparticles that are chemically reacting, over a stretching permeable sheet by generating heat and nanoparticle volume fraction. The perturbation technique to determine the impact of the hybrid nanoparticles' shape factor on the convective heat and mass characteristics of non-miscible liquids in an inclined duct was employed by Ananth Subray *et al.* [55]. Saranya and Al-Mdallal [56] investigated the role of nanoparticle shape in the radial flow of *Al$_2$O$_3$* silicon oil nanofluid around a rotating disc. Results from the magnetic field and radiation energy were also considered and in this study were utilized five different shaped *Al$_2$O$_3$* nanoparticles, including sphere, brick, cylinder, platelet, and blade. The shape impacts of copper (*Cu*) nanoparticles on the three-dimensional magnetohydrodynamic (MHD) nanofluid's ability to conduct heat was studied by Zubair *et al.* [57]. The dynamics of a three-dimensional rotating Maxwell nanoliquid across a stretching sheet with different shape factors using water as a base fluid with (*Cu*) nanoparticles was modeled by Akbar *et al.* [58].

Motivated by the earlier studies and review of the published literature (Chamkha *et al.* [59], Umavathi *et al.* [60], Vijayalakshmi and Srinivas [28], Kumar and Suripeddi [11]) and numerous applications of such a study, the main objective of the present work is to mathematically model and to understand the combined influences of velocity and thermal slips on the pulsating MHD flow of a nanofluid, with different shape factors of the nanoparticles, in a porous space of two immiscible liquids. To the best of the authors' knowledge, the simultaneous effects of these quantities in the presence of a magnetic field, Joule heating, viscous dissipation, Darcy dissipation, thermal radiation, and flow of nanofluids through a porous medium have not been analyzed. Hence, this problem is investigated. *Al$_2$O$_3$-H$_2$O* and *Cu-H$_2$O* are considered in region-I and II respectively. Velocity, temperature, volume fraction, shape factor, and Nusselt number are illustrated graphically. Furthermore, profiles of the temperature of the liquid and rate of heat transfer are examined with four different shapes of the nanoparticles (bricks, cylinder, platelets, and spherical) and are presented graphically. Shear stress, and mass flux as a function of various parameters are shown in a tabular form. The effects of significant parameters on flow and heat transfer characteristics are investigated and graphically represented. As a novelty, the effects of different shape factors are investigated. This model can be utilized for transporting nanofluids in a two-immiscible channel with different nanoparticles and in drug delivery systems.

2. Mathematical formulation and solution

Consider a pulsatile and fully developed unsteady MHD flow of two immiscible nanofluids in a horizontal porous channel under the influence of nanoparticles shape factor on energy equation. Figure 1 describes the flow configuration of the proposed model with the *x*-axis chosen along the flow direction and the *y*-axis perpendicular to the walls of the channel.
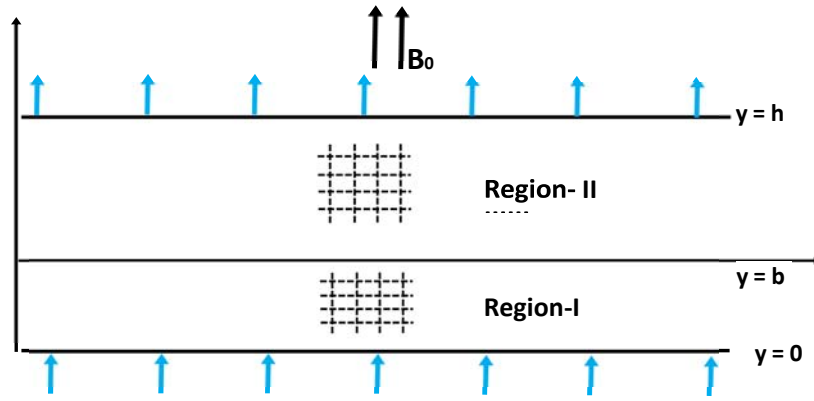
Fig.1. Flow geometry.

It is considered that region-I is $0 \le y \le b$ and $b \le y \le h$ represents region-II. The fluid is assumed to be injected into the channel through the injection wall, which is placed at $y=0$ with the velocity v_0 and sucked out from the channel with the same velocity v_0 through the suction wall at $y=h$. Perpendicular to the walls, a uniform magnetic field of strength B_0 is applied. The magnetic Reynolds number is so low that the impact of the magnetic field induced by the fluid flow can be neglected. The permeability of the porous medium, viscous dissipation, Darcy dissipation, Ohmic effect, and thermal radiation have been taken into consideration. We have contains two immiscible liquid layers in porous spaces of regions I and II. The lower and upper regions are occupied by Al_2O_3-water and Cu-water with different densities, ρ_{1nf}, ρ_{2nf} two different viscosities μ_{1nf}, μ_{2nf} different electrical conductivities $\sigma_{1nf}, \sigma_{2nf}$ of lower and upper regions of the channel, respectively. The flow situation is analysed for both the velocity and thermal slips at the walls. Since the flow has fully developed, which means $\frac{\partial u}{\partial x} = 0$, i.e., the velocity, u is solenoidal which results in $\frac{\partial v}{\partial y} = 0$. Thus, v does not change in any section of the channel and it will be zero at the channel walls in such way that $v = 0$ at any position of the channel. Therefore, the momentum equation along the y-direction is $\frac{\partial p}{\partial y} = 0$. The flow is subjected to an oscillatory pressure gradient of the form:

$$\frac{\partial p}{\partial x} = \left(\frac{\partial p}{\partial x} \right)_s + \varepsilon \left(\frac{\partial p}{\partial x} \right)_O e^{it},$$

$$\left(\frac{\partial p}{\partial x} \right)_s, \left(\frac{\partial p}{\partial x} \right)_O,$$

(2.1)

are the gradients of pressure in the steady and unsteady terms, respectively In view of these suppositions, the governing liquid flow equations, [27] are:

Region-I

$$\rho_{1nf} \left(\frac{\partial u_1}{\partial t} + v \frac{\partial u_1}{\partial y} \right) = -\frac{\partial p}{\partial x} + \mu_{1nf} \frac{\partial^2 u_1}{\partial y^2} - \sigma_{1nf} B_0^2 u_1 - \frac{\mu_{1nf}}{k_{1p}} u_1,$$

(2.2)

$$\left(\rho C_p\right)_{1nf}\left(\frac{\partial T_1}{\partial t}+v\frac{\partial T_1}{\partial y}\right)=k_{1nf}\frac{\partial^2 T_1}{\partial y^2}+\mu_{1nf}\left(\frac{\partial u_1}{\partial y}\right)^2-\frac{\partial q_r}{\partial y}-\sigma_{1nf}B_0^2u_1^2+\frac{\mu_{1nf}}{k_{1p}}u_1^2. \tag{2.3}$$

Region-II

$$\rho_{2nf}\left(\frac{\partial u_2}{\partial t}+v\frac{\partial u_2}{\partial y}\right)=-\frac{\partial p}{\partial x}+\mu_{2nf}\frac{\partial^2 u_2}{\partial y^2}-\sigma_{2nf}B_0^2u_2-\frac{\mu_{2nf}}{k_{2p}}u_2, \tag{2.4}$$

$$\left(\rho C_p\right)_{2nf}\left(\frac{\partial T_2}{\partial t}+v\frac{\partial T_2}{\partial y}\right)=k_{2nf}\frac{\partial^2 T_2}{\partial y^2}+\mu_{2nf}\left(\frac{\partial u_2}{\partial y}\right)^2-\frac{\partial q_r}{\partial y}-\sigma_{2nf}B_0^2u_2^2+\frac{\mu_{2nf}}{k_{2p}}u_2^2, \tag{2.5}$$

q_r^* represents the radiative heat flux. The radiative heat flux q_r^*, using the Rosseland approximation, is

$$q_r^*=-\frac{4\sigma^*}{3k^*}\frac{\partial T^{*4}}{\partial y^*}, \tag{2.6}$$

here $\sigma^*=\left(5.6697\times10^{-8}\,Wm^{-2}K^{-4}\right)$ and k^* represents the Stefan-Boltzmann constant and Rosseland mean absorption coefficient, respectively. Expressing T^* as a linear function of T, under the assumption that within the liquid the temperature variations are small, we get:

$$T^{*4}\cong 4T_1^3T^*-3T_1^4$$

Table 1. Thermal physical properties of nanofluids [11, 27, 55].

Property	Water	*Ag*	*Cu*	*Al₂O₃*	*TiO₂*
density (*kg/m³*)	*997.1*	*10500*	*8933*	*3970*	*4250*
specific heat (*J/kgK*)	*4179*	*235*	*385*	*765*	*686.2*
thermal conductivity (*W/mK*)	*0.613*	*429*	*400*	*40*	*8.9538*
electrical conductivity (*Ωm*)ᴵ	*0.05*	*6.30 × 10⁷*	*5.96 × 10⁷*	*1 × 10⁻¹⁰*	*1 × 10⁻¹²*

The nanoliquid of effective density is expressed as [27]:

$$\rho_{1nf}=\left(1-\phi\right)\rho_{1f}+\phi\rho_{1s}, \qquad \mu_{1nf}=\frac{\mu_{1f}}{\left(1-\phi\right)^{2.5}},$$

$$\left(\rho C_p\right)_{1nf}=\left(1-\phi\right)\left(\rho C_p\right)_{1f}+\phi\left(\rho C_p\right)_{1s},$$

$$\frac{k_{1nf}}{k_{1f}}=\frac{k_{1s}+2k_{1f}-2\phi\left(k_{1f}-k_{1s}\right)}{k_{1s}+2k_{1f}+\phi\left(k_{1f}-k_{1s}\right)},$$

$$\frac{\sigma_{1nf}}{\sigma_{1f}} = 1 + \frac{3\phi\left(\frac{\sigma_{1s}}{\sigma_{1f}} - 1\right)}{\left(\frac{\sigma_{1s}}{\sigma_{1f}} + 2\right) - \left(\frac{\sigma_{1s}}{\sigma_{1f}} - 1\right)\phi}.$$

The influences of shape factor nanoparticle, the nanofluid thermal conductivity k_{nf} is characterized as follows [58]:

$$\frac{k_{1nf}}{k_{1f}} = \frac{(m-1)\phi\left(k_{1s} - k_{1f}\right) + k_{1s} - (1-m)k_{1f}}{k_{1s} - (1-m)k_{1f} - \phi\left(k_{1s} - k_{1f}\right)}, \tag{2.7}$$

where m is the shape factor for which the numerical values for various shapes are presented in Tab.1 (Hamilton Crosser's model [63]). It should be noted that the sphericity (the ratio of the sphere's surface area to the surface area of real particles with equal volumes) is reflected in the shape factor as $m=3/a$. The results for shape factor of spherical, brick, cylinder, platelet, column, blade, and lamina, respectively, are shown in Tab.2. When the nanoparticle's shape factor is $m=3$, then the Hamilton Crosser's model is transformed into a Maxwell model. The non-dimensional boundary conditions are as follows [29, 39, 45]:

$$u_1^*(0) = \lambda_1 \frac{\partial u_1^*}{\partial y}(0), \quad u_2^*(h) = -\lambda_1 \frac{\partial u_2^*}{\partial y}(h), \quad u_1^*(b) = u_2^*(b),$$

$$\mu_{1nf} \left.\frac{\partial u_1^*}{\partial y}\right|_{y=b} = \mu_{2nf} \left.\frac{\partial u_2^*}{\partial y}\right|_{y=b},$$

$$\tag{2.8}$$

$$T_1^*(0) = T_{w1} + k_{1nf} \frac{\partial T_1^*}{\partial y}(0), \quad T_2^*(h) = T_{w2} - k_{2nf} \frac{\partial T_2^*}{\partial y}(h)$$

$$k_{1nf} \left.\frac{\partial T_1^*}{\partial y}\right|_{y=b} = k_{2nf} \left.\frac{\partial T_2^*}{\partial y}\right|_{y=b}$$

Table 2. Various shape factors [56].

Shape factors	spherical	brick	cylinder	platelet	column	Blade	lamina
shapes							
shape factor values	3	3.7	4.8	5.7	6.3698	8.6	16.1576
sphericity	1	0.811	0.625	0.526	0.471	0.348	0.185

The non-dimensional quantities are [27]:

$$x = \frac{x^*}{h}, \quad y = \frac{y^*}{h}, \quad b = \frac{b^*}{h}, \quad u_i = \frac{u_i^* \omega}{A}, \quad t = t^* \omega, \quad P = \frac{P^*}{A\rho_{1f} h}, \quad H = h\sqrt{\frac{\omega}{\gamma_{1f}}}, \quad \mathrm{Re} = \frac{v_0 h}{\gamma_{1f}},$$

$$A_1 = \frac{\rho_{1nf}}{\rho_{1f}}, \quad A_2 = \frac{\mu_{1nf}}{\mu_{1f}}, \quad A_3 = \frac{(\rho C_p)_{1nf}}{(\rho C_p)_{1f}}, \quad A_4 = \frac{k_{1nf}}{k_{1f}}, \quad A_5 = \frac{\sigma_{1nf}}{\sigma_{1f}}, \quad u_{i1} = \frac{u_{i1}^* \omega}{A}, \quad u_{i2} = \frac{u_{i2}^* \omega}{A},$$

$$\alpha_{nf} = \frac{\rho_{1nf}}{\rho_{2nf}}, \quad M_1 = B_0 h\sqrt{\frac{\sigma_{1nf}}{\mu_{1f}}}, \quad \mathrm{Pr} = \frac{\mu_{1f}}{k_{1f}}(C_p)_{1f}, \quad Rd = \frac{4\sigma^*}{k^* k_{1f}} T_1^3, \quad \beta_{nf} = \frac{\mu_{1nf}}{\mu_{2nf}},$$

$$\gamma_{nf} = \frac{\sigma_{1nf}}{\sigma_{2nf}}, \quad k_{nf} = \frac{k_{2nf}}{k_{1nf}}, \quad \theta_i = \frac{T_i^* - T_0}{T_{w_1} - T_{w_2}}, \quad Da = \frac{k_{1p}}{h^2}, \quad k_p = \frac{k_{2p}}{k_{1p}},$$

$$E_c = \frac{A^2}{\omega^2 (C_p)_{1f} (T_{w_1} - T_{w_2})}, \quad M_2 = B_0 h\sqrt{\frac{\sigma_{2nf}}{\mu_{2f}}} \left(M_2 = M_1 \sqrt{\frac{\beta_{nf}}{\gamma_{nf}}} \right).$$

Using the above non-dimensional quantities, the governing equations become:

Region-I

$$A_1 \left[H^2 \frac{du_1}{dt} + R \frac{du_1}{dy} \right] = -H^2 \frac{dp}{dx} + A_2 \frac{d^2 u_1}{dy^2} - A_5 M_1^2 u_1 - \frac{A_2}{Da} u_1,$$

$$\tag{2.9}$$

$$A_1 \alpha_{nf} \beta_{nf} \left[H^2 \frac{du_2}{dt} + R \frac{du_2}{dy} \right] = -H^2 \beta_{nf} \frac{dp}{dx} + A_2 \frac{d^2 u_2}{dy^2} - A_5 M_2^2 u_2 - \frac{A_2}{Da \, kp} u_2.$$

Region-II

$$A_3 \mathrm{Pr} \left[H^2 \frac{d\theta_1}{dt} + R \frac{d\theta_1}{dy} \right] = \left(A_4 + \frac{4}{3} Rd \right) \frac{d^2 \theta_1}{dy^2} + A_2 Ec \mathrm{Pr} \left(\frac{du_1}{dy} \right)^2,$$

$$\left(A_5 Ec \mathrm{Pr} M_1^2 + \frac{A_2 Ec \mathrm{Pr}}{Da} \right) u_1^2 + A_3 (\alpha Cp)_{nf} \mathrm{Pr} \beta_{nf} \left[H^2 \frac{d\theta_2}{dt} + R \frac{d\theta_2}{dy} \right] = \tag{2.10}$$

$$= \left(k_{nf} A_4 \beta_{nf} + \frac{4}{3} Rd \beta_{nf} \right) \frac{d^2 \theta_2}{dy^2} + A_2 Ec \mathrm{Pr} \left(\frac{du_2}{dy} \right)^2 + \left(A_5 Ec \mathrm{Pr} M_2^2 + \frac{A_2 Ec \mathrm{Pr}}{kpDa} \right) u_2^2.$$

The hydrodynamic, thermal boundary, and interface conditions are [29, 37, 43]:

$$u_1(0) = \alpha^* \frac{\partial u_1}{\partial y}(0), \quad u_2(h) = -\alpha^* \frac{\partial u_2}{\partial y}(h), \quad u_1(b) = u_2(b),$$

$$\mu_{1nf} \frac{\partial u_1}{\partial y}\bigg|_{y=b} = \mu_{2nf} \frac{\partial u_2}{\partial y}\bigg|_{y=b},$$

(2.11)

$$\theta_1(0) = \beta^* \frac{\partial \theta_1}{\partial y}(0), \quad \theta_2(1) = 1 - k_{nf}\beta^* \frac{\partial \theta_2}{\partial y}(1),$$

$$k_{1nf} \frac{\partial \theta_1}{\partial y}\bigg|_{y=b} = k_{2nf} \frac{\partial \theta_2}{\partial y}\bigg|_{y=b},$$

where $\alpha^* = \dfrac{\lambda_1}{h}, \beta^* = \dfrac{A_4 k_{1f}}{h}$ are the slip parameters of velocity and temperature distributions of both regions respectively. The governing equation (2.15)-(2.18) along with equation (2.19) can be solved [56, 57, 59]

$$u_i = u_{i1} + \varepsilon u_{i2} e^{it},$$

(2.12)

$$\theta_i = \theta_{i1} + \varepsilon \theta_{i2} e^{it},$$

by using equation .(2.11) the boundary conditions are as follows:

$$u_{11}(0) = \alpha^* \frac{\partial u_{11}}{\partial y}(0), \quad u_{12}(0) = \alpha^* \frac{\partial u_{12}}{\partial y}(0),$$

$$u_{21}(1) = -\alpha^* \frac{\partial u_{21}}{\partial y}(1), \quad u_{22}(1) = -\alpha^* \frac{\partial u_{22}}{\partial y}(1),$$

(2.13)

$$u_{11}(b) = u_{21}(b), \quad u_{12}(b) = u_{22}(b),$$

$$\mu_{1nf} \frac{\partial u_{11}}{\partial y}\bigg|_{y=b} = \mu_{2nf} \frac{\partial u_{21}}{\partial y}\bigg|_{y=b}, \quad \mu_{1nf} \frac{\partial u_{12}}{\partial y}\bigg|_{y=b} = \mu_{2nf} \frac{\partial u_{22}}{\partial y}\bigg|_{y=b}.$$

$$\theta_{11}(0) = \beta^* \frac{\partial \theta_{11}}{\partial y}(0), \quad \theta_{12}(0) = \beta^* \frac{\partial \theta_{12}}{\partial y}(0),$$

(2.14)

$$\theta_{21}(1) = 1 - k_{nf}\beta^* \frac{\partial \theta_{21}}{\partial y}(1), \quad \theta_{22}(1) = -k_{nf}\beta^* \frac{\partial \theta_{22}}{\partial y}(1),$$

$$\theta_{11}(b) = \theta_{21}(b), \quad \theta_{12}(b) = \theta_{22}(b),$$

<div align="right">(cont.2.14)</div>

$$k_{1nf} \left.\frac{\partial \theta_{11}}{\partial y}\right|_{y=b} = k_{2nf} \left.\frac{\partial \theta_{21}}{\partial y}\right|_{y=b}, \quad k_{1nf} \left.\frac{\partial \theta_{12}}{\partial y}\right|_{y=b} = k_{2nf} \left.\frac{\partial \theta_{22}}{\partial y}\right|_{y=b}.$$

The governing flow equations are reduced to steady and unsteady components as follows:

Region-I

$$\frac{d^2 u_{11}}{dy^2} - Rp_1 \frac{du_{11}}{dy} - p_2 u_{11} = p_3, \quad \frac{d^2 u_{12}}{dy^2} - Rp_1 \frac{du_{12}}{dy} - p_7 u_{12} = p_8,$$

<div align="right">(2.15)</div>

$$\frac{d^2 u_{21}}{dy^2} - Rp_{13} \frac{du_{21}}{dy} - p_{12} u_{21} = p_{14}, \quad \frac{d^2 u_{22}}{dy^2} - Rp_{13} \frac{du_{22}}{dy} - p_{18} u_{22} = p_{19}.$$

Region-II

$$\frac{d^2 \theta_{11}}{dy^2} - Rp_{95} \frac{d\theta_{11}}{dy} = p_{96} \left(\frac{du_{11}}{dy}\right)^2 - p_{97} u_{11}^2,$$

$$\frac{d^2 \theta_{12}}{dy^2} - Rp_{95} \frac{d\theta_{12}}{dy} - p_{98}\theta_{12} = 2p_{96} \left(\frac{du_{11}}{dy}\frac{du_{12}}{dy}\right) - 2p_{97} u_{11} u_{12},$$

<div align="right">(2.16)</div>

$$\frac{d^2 \theta_{21}}{dy^2} - Rp_{99} \frac{d\theta_{21}}{dy} = p_{100} \left(\frac{du_{21}}{dy}\right)^2 - p_{101} u_{21}^2,$$

$$\frac{d^2 \theta_{22}}{dy^2} - Rp_{99} \frac{d\theta_{22}}{dy} - p_{102}\theta_{22} = 2p_{100} \left(\frac{du_{21}}{dy}\frac{du_{22}}{dy}\right) - 2p_{101} u_{21} u_{22}.$$

3. Solution of the problem

Region-I

$$u_{11} = C_1 e^{p_4 y} + C_2 e^{p_5 y} - p_6, \quad u_{12} = C_3 e^{p_9 y} + C_4 e^{p_{10} y} - p_{11},$$

$$\theta_{11} = C_9 + C_{10} e^{Rp_{95} y} + p_{105} e^{2 p_4 y} + p_{106} e^{2 p_5 y} + p_{107} e^{(p_4 + p_5) y} - p_{108} y^2 +$$
$$+ p_{109} e^{p_5 y} + p_{110} e^{p_6 y},$$

<div align="right">(3.1)</div>

$$\theta_{12} = C_{11} e^{p_{111} y} + C_{12} e^{p_{112} y} + p_{126} e^{(p_4 + p_9) y} + p_{127} e^{(p_4 + p_{10}) y} + p_{128} e^{(p_5 + p_9) y} +$$
$$+ p_{129} e^{(p_5 + p_{10}) y} + p_{130} e^{p_4 y} + p_{131} e^{p_5 y} + p_{132} e^{p_9 y} + p_{133} e^{p_{10} y} + p_{134}.$$

Region-II

$$u_{21} = C_5 e^{p_{15}y} + C_6 e^{p_{16}y} - p_{17}, \quad u_{22} = C_7 e^{p_{20}y} + C_8 e^{p_{21}y} - p_{22},$$

$$\theta_{21} = C_{13} + C_{14} e^{Rp_{99}y} + p_{137} e^{2p_{15}y} + p_{138} e^{2p_{16}y} + p_{139} e^{(p_{15}+p_{16})y} +$$
$$-p_{140} y^2 + p_{141} e^{p_{15}y} + p_{142} e^{p_{16}y}$$

$$\theta_{22} = C_{15} e^{p_{143}ay} + C_{16} e^{p_{144}ay} + p_{143} e^{(p_{15}+p_{20})y} + p_{144} e^{(p_{15}+p_{21})y} + p_{145} e^{(p_{16}+p_{20})y} +$$

$$+ p_{146} e^{(p_{16}+p_{21})y} + p_{147} e^{p_{15}y} + p_{148} e^{p_{16}y} + p_{149} e^{p_{20}y} + p_{150} e^{p_{21}y} + p_{151}$$

(3.2)

4. Shear stress and rate of heat transfer

Skin friction and flow Nusselt numbers are two characteristics that are very important for engineering applications. The skin friction basically corresponds to the velocity boundary layer, while the Nusselt number corresponds to the thermal boundary layer. Shear stress is a measurement of the resistance provided by the fluid surface as it flows. The fluid viscosity is the main cause of it. The Nusselt number is essentially a ratio of heat transfer due to conduction to heat transfer due to convection. The Nusselt number thus reveals how much heat transmission is improved as a result of fluid motion. So, the definitions of shear stress and rate of heat transfer are as follows [61, 62]:

$$\tau_1 = \left(\frac{A_2}{Re} \frac{du_1}{dy} \right)_{y=0,1},$$

$$\tau_2 = \left(\frac{A_2}{\beta_{nf} Re} \frac{du_2}{dy} \right)_{y=0,1}.$$

(4.1)

The rate of heat transfer is given by

$$Nu = A_4 \left[\left(\frac{d\theta_1}{dy} \right)_{y=0,1} + \varepsilon e^{it} \left(\frac{d\theta_2}{dy} \right)_{y=0,1} \right].$$

(4.2)

5. Mass flux

The flow rate in the regions I and II are as follows:

$$Q_1 = \int_0^b u_{11} dy + \varepsilon \left[\int_0^1 u_{12} dy \right] e^{it}, \qquad Q_2 = \int_0^b u_{21} dy + \varepsilon \left[\int_0^1 u_{22} dy \right] e^{it}.$$

(5.1)

6. Results and discussion

An analytical method is used to calculate the two-layered oscillatory MHD nanofluid flow with various shape factors by employing the regular perturbation method for numerous germane parameters. Aluminum oxide and Copper were dispersed into testing fluid which was selected water as a base fluid in Region-I and II respectively. Darcy's law for porous media enables us to understand equations in simpler forms. The shape factor effects on the thermal conduct of nanoparticles inside a permeable space were investigated. Influence of permeability, Hartmann number, Radiation parameter, shape factor, volume fraction, viscous and Darcy dissipation, of both Al_2O_3-H_2O, and Cu-H_2O have been depicted graphically in Figs.2-31. In the profiles, the dashed line and solid line represent the slip and no-slip effects respectively. Furthermore, for plotting the graphs of Figs (2-31) values chosen for different parameters are: $H=4$, $P_0=2$, $P_s=2.5$, $M_1=1$, $M_2=2$, $R=2$, $D_a=0.05$, $k_p=2$, $Rd=0.1$, $Ec=0.1$, $b=0.25$, $Pr=6.2$, $m=3$, $t=\pi/4$ and $\varphi=0.05$. From Fig.2 display that the influence of velocity profiles of different parameters like b, Da, kp, M_1, M_2. It is evident from Fig.2 that with the rise of b, the fluid velocity falls. As Da rises, velocity is enhanced due to that the nanoparticles can affect the porosity and tortuosity of a medium, which leads to changes in effective permeability. The pressure gradient or viscosity of the fluid can increase as the Darcy number increases, but the permeability remains relatively constant or changes at a slower rate. This leads to the flow rate rising, resulting in increased velocities as shown in Fig.3. When the permeability ratio increases, it means that the medium offers less resistance to flow, resulting in an enhancement in velocity. Higher flow rates and velocities arise from the fluid flowing more easily through the porous media as illustrated in Fig.4. As the Hartmann number of the two regions increases, the velocity reduces as can be seen in Fig.5. It is justified because as the Hartmann number raises, the Lorentz forces become more significant compared to the other forces governing the flow. The stronger magnetic field creates a stronger resistance to the fluid motion, impeding its flow through the porous medium. Consequently, the velocity decreases and the Lorentz forces act as an additional drag force on the fluid, effectively dampening the fluid motion and reducing the overall velocity.

To gain insight of Fig.6-11 are brought to see the influence of shape factors (sphere, bricks, cylinder and platelets) are sequenced as *cylinder<brick<platelets<sphere* on temperature profiles. The flow pattern, flow resistance, and heat transfer properties of a porous media can be affected by shape factors such as spheres, cylinders, bricks, and platelets. These shape factors are able to have an impact on the temperature distribution throughout the channel. One can observe from Fig.6 that, with the raise of b, the liquid of the temperature is increased. The Darcy number describes the flow characteristics and resistance within the porous medium, and an increase in the Darcy number indicates a higher flow rate or pressure gradient relative to the permeability of the porous medium. Increases in the Darcy number typically indicate increased flow rates or pressure gradients inside the channel. However, the exact influence on temperature would be determined by the interaction of heat transmission processes, shape parameters, nanoparticle characteristics, and the unique circumstances of two regions where the fluid's temperature falls that was presented in Fig.7. Figure 8 shows that as k_p increases, the temperature of the fluid decreases. This is because an increase in the permeability of the medium suggests reduced resistance due to the porous matrix present in the medium. Figure 9 depicts the distribution of the temperature for air, carbon disulfide, Freon, and water. It is observed that liquid temperature falls with a rise Pr, which results in a low thermal penetration causing a decrease in the temperature distribution. The Rd defines the relative contribution of heat conduction to thermal radiation transfers. From Fig.10 it is observed that a rise in Rd leads to an increase in the temperature of the liquid. The sphere-shaped nanoparticle of Al_2O_3 and Cu with base fluid water in region-I and II have a greater temperature of the liquid when Rd rises. The evaluation of the results reveals that the thermal conductivity has a significant impact on sphere-shaped nanoparticles in the flow fields of Al_2O_3-water and Cu-water nanofluids. Figure 11 shows that the fluid's temperature drops as Ec increases. The ratio of kinetic energy to thermal energy in a flowing fluid is denoted by the Eckert number Ec. An increase in the Eckert number indicates enhanced convective heat transfer due to increased kinetic energy. Because of the improved convective heat transmission, the temperature within the channel rises.

Graphs
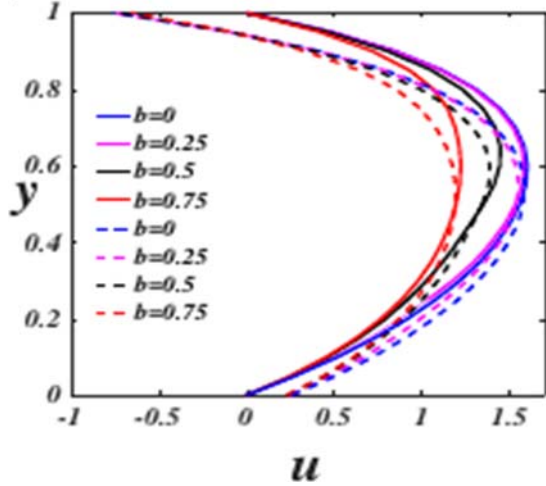
Fig.2. Velocity profile of *b*.
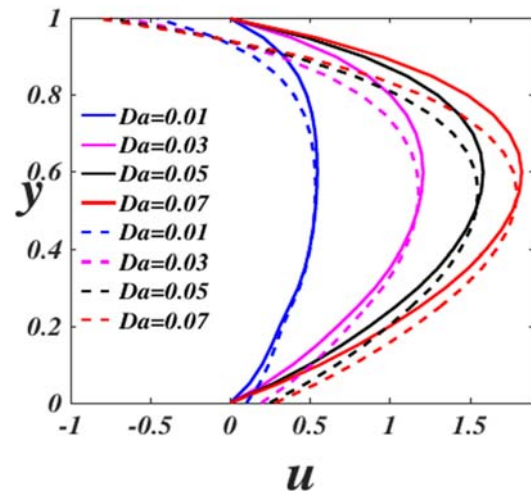
Fig.3. Velocity profile of *Da*.
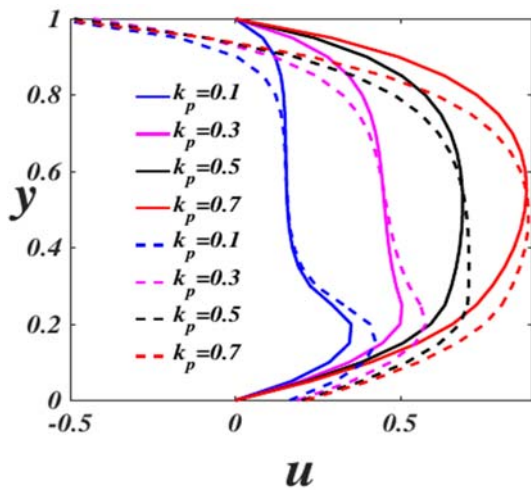
Fig.4. Velocity profile of permeability.
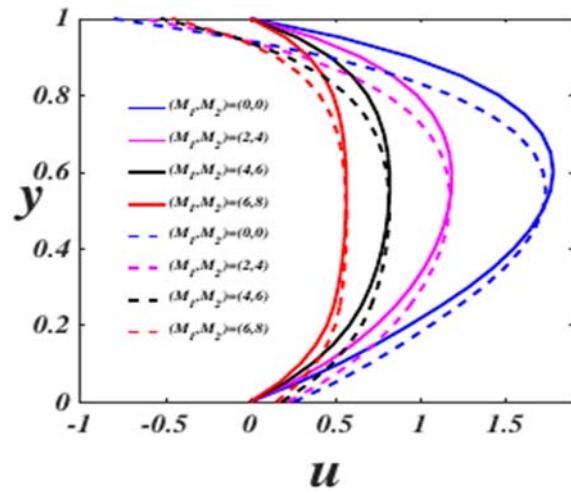
Fig.5. Velocity profile of Hartmann number.
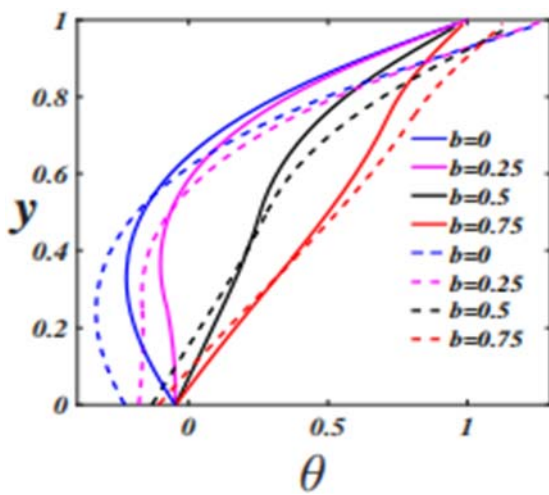
Fig.6. Temperature profile of *b*.
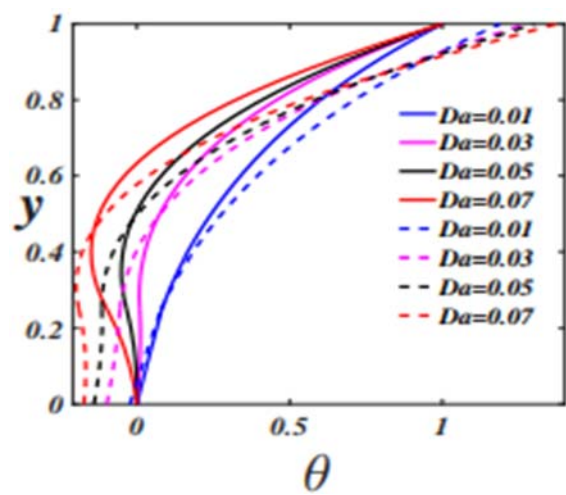
Fig.7.Temperature profile of *Da*.
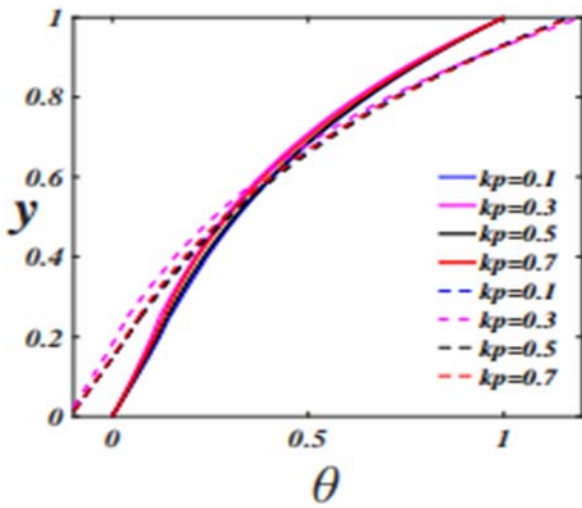
Fig.8. Temperature profile of k_p.
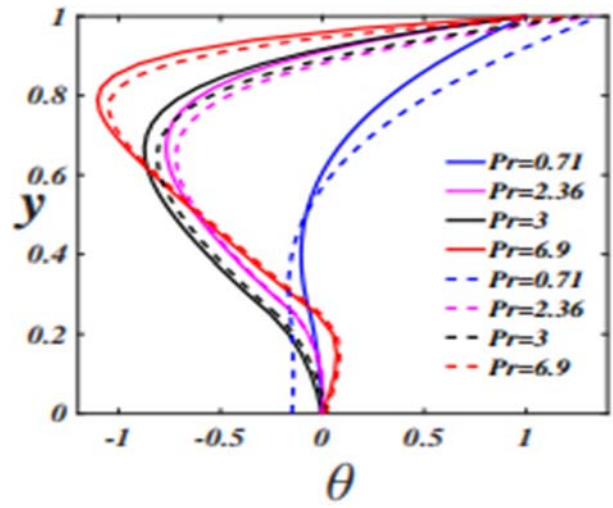
Fig.9.Temperature profile of *Pr*.
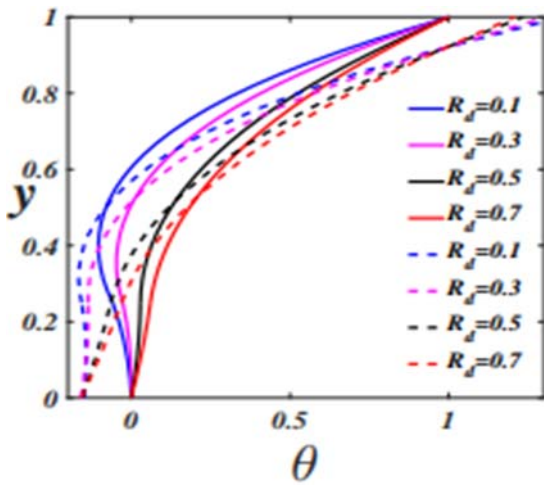
Fig.10. Temperature profile of *Rd*.
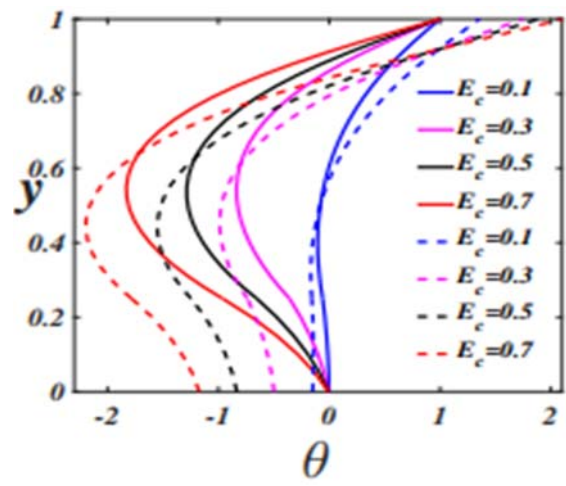
Fig.11.Temperature profile of *Ec*.
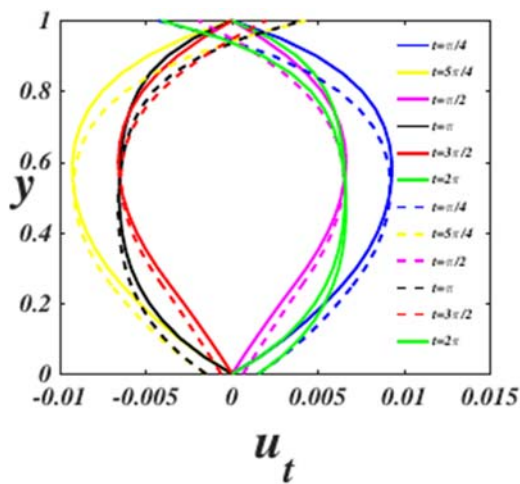
Fig.12. Unsteady velocity profile.
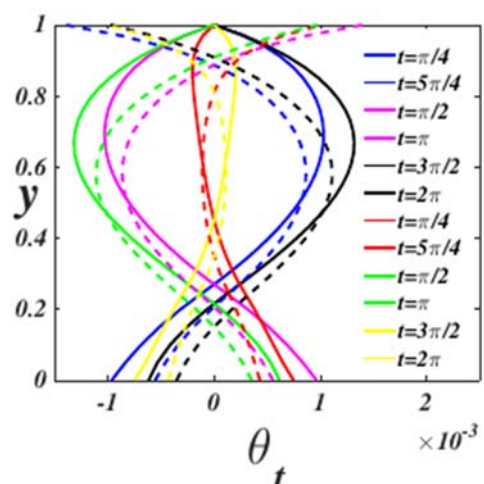
Fig.13. Unsteady temperature profile.
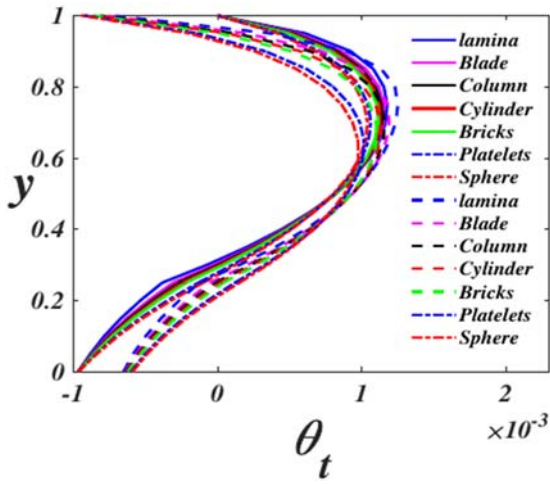
Fig.14. Unsteady shape factor profile.
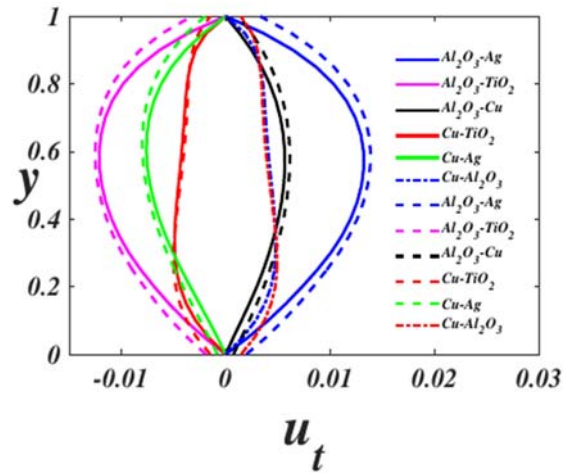
Fig.15. Unsteady velocity profile of different nanoparticles.
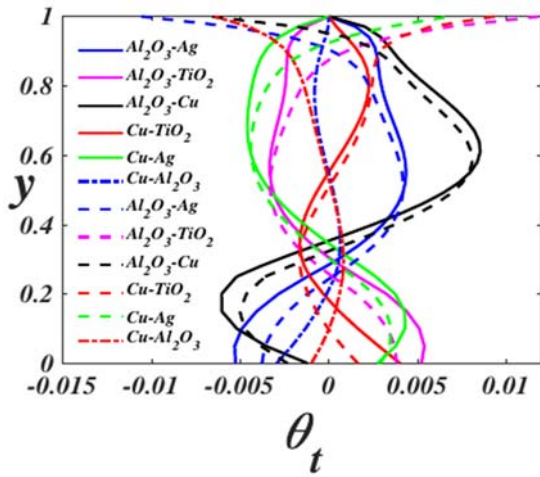
Fig.16. Unsteady temperature of different nanoparticles.
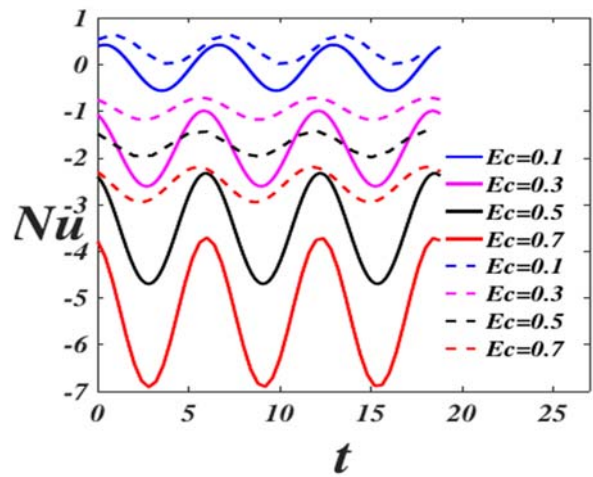
Fig.17. Lower region of Nu with Ec.
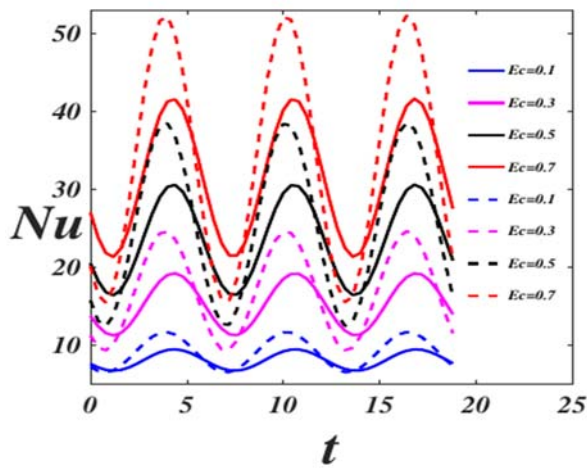
Fig.18. Upper region of Nu with Ec.
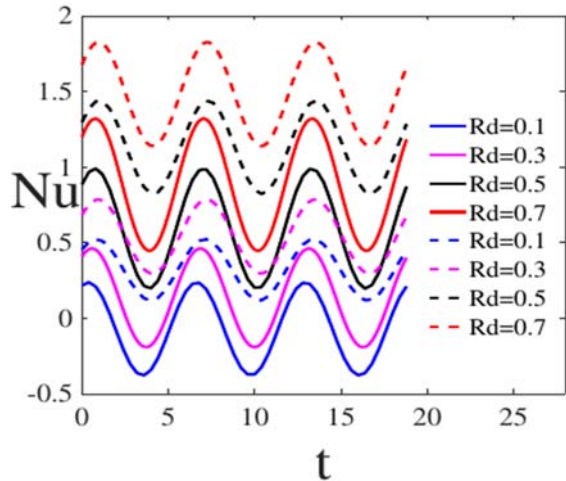
Fig.19. Lower region of Nu with Rd.
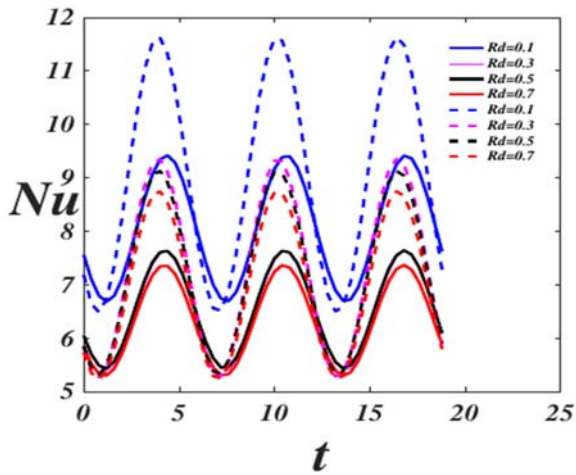
Fig.20. Upper region of *Nu* with *Rd.*
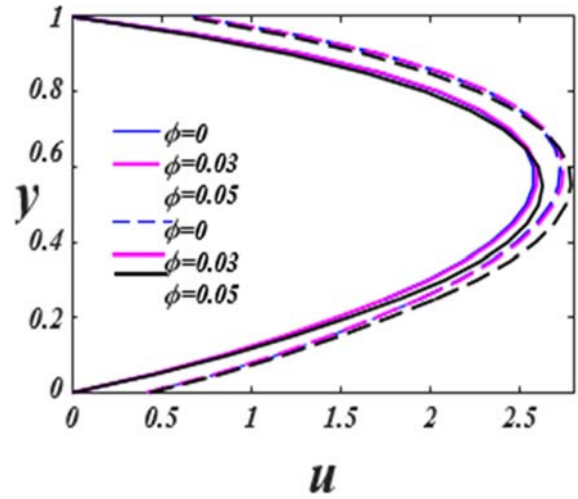
Fig.21. Velocity profile of volume fraction.
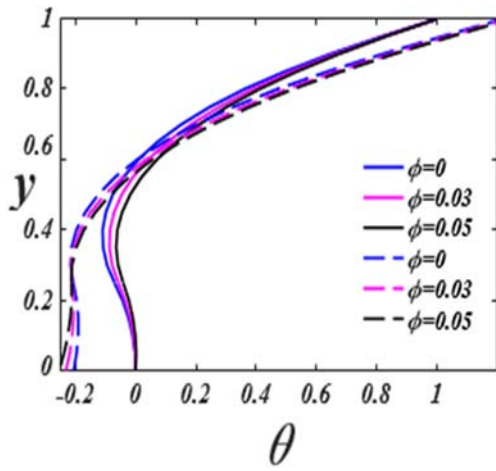
Fig.22. Temperature profile of ϕ.
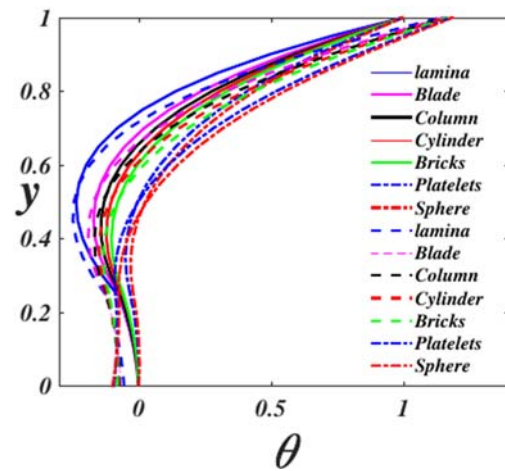
Fig.23. Temperature profile of different shape factors.
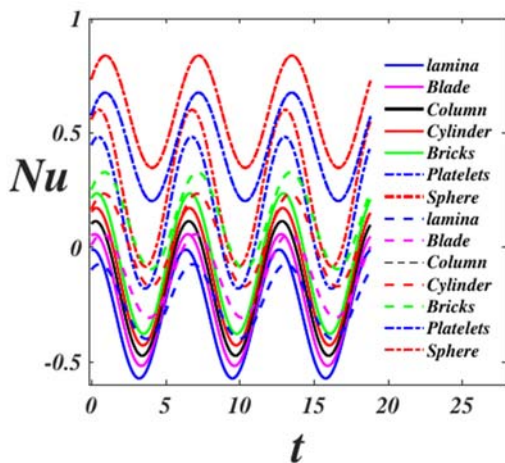
Fig.24. Lower region of *Nu* with different shape factors.
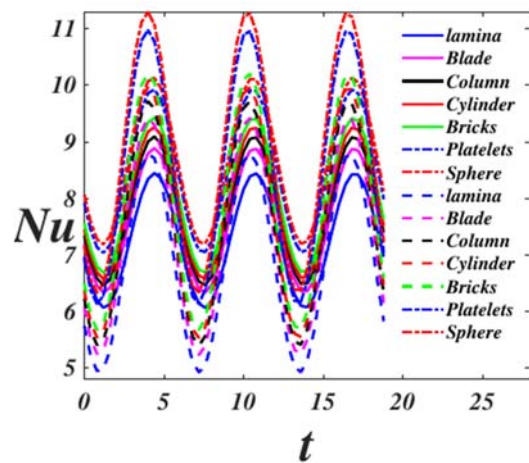
Fig.25. Upper region of *Nu* with different shape factors.
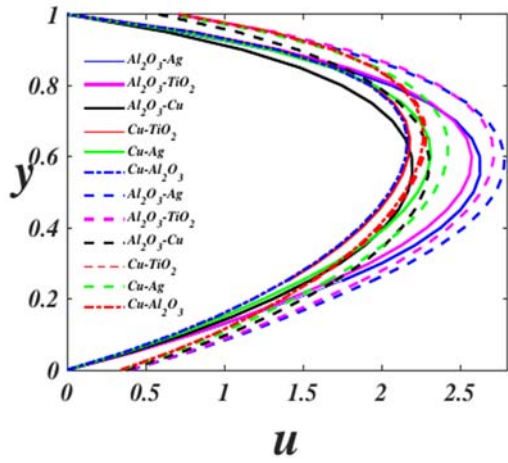
Fig.26. Velocity profile of different nanoparticles.
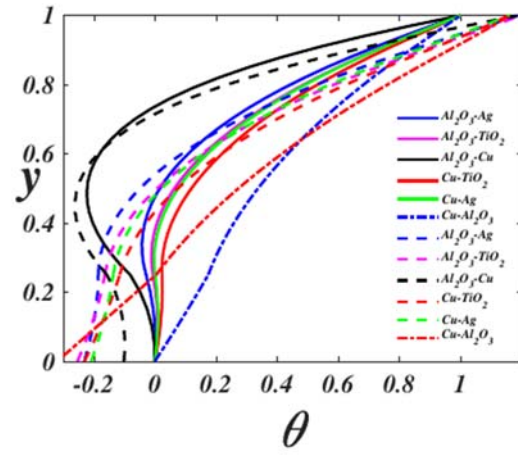
Fig.27. Temperature profile of different nanoparticles.
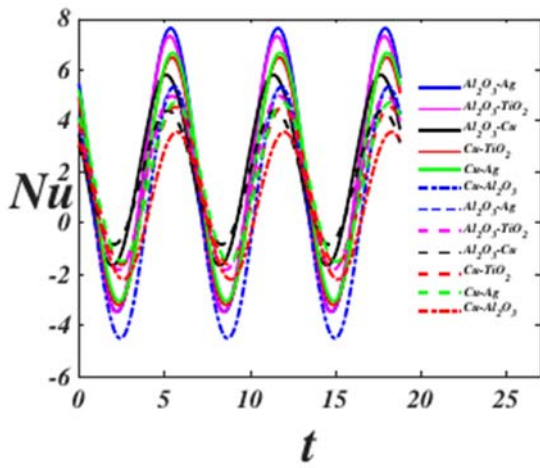
Fig.28. Lower region of *Nu* with different nanoparticles.
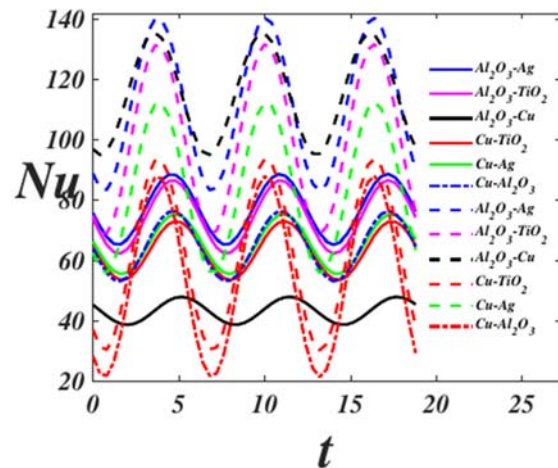
Fig.29. Upper region of *Nu* with different nanoparticles.
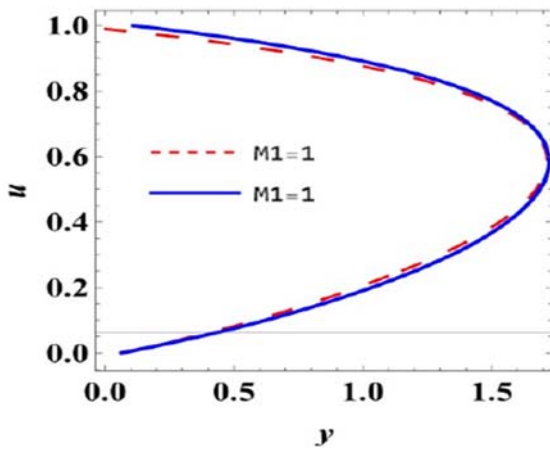
Fig.30.Comparative study of slip velocity with Hartmann number.
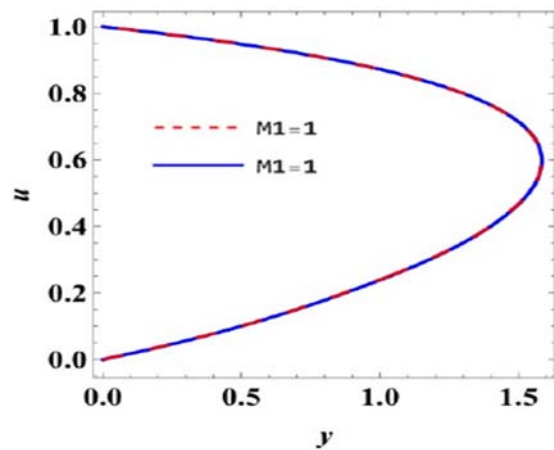
Fig.31. Comparative study of no-slip velocity with Hartmann number.

Table 3. Variation of shear stress with $\alpha^*=0.05$ (slip).

t	b	D_a 0.01	0.03	0.05	k_p 0.1	0.3	0.5	Re 0	1	3
0	0.25	274.20	137.45	47.893	221.48	122.30	80.737	22.430	33.615	65.886
π/4		273.43	137.29	47.91	220.25	121.61	80.29	22.434	33.628	65.924
π/2		271.16	136.630	47.716	218.912	120.861	79.811	22.335	33.487	65.638
0	0.5	169.93	20.97	10.976	1722.5	86.259	37.433	5.0798	5.949	16.5976
π/4		169.59	20.98	11.00	1718.4	85.95	37.28	5.0965	5.9638	16.6337
π/2		168.67	20.91	10.97	1709.1	85.44	37.07	5.076	5.9556	16.5926
0	0.75	55.780	5.722	4.929	4899.5	360.305	66.027	10.388	5.3609	9.4909
π/4		55.468	5.668	4.9456	4886.2	358.77	65.698	10.3294	5.3203	9.4992
π/2		55.113	5.613	4.9457	4859.9	356.705	65.328	10.233	5.2620	9.4750

Table 4. Variation of shear stress with $\alpha^*=0$ (no-slip).

t	b	D_a 0.01	0.03	0.05	k_p 0.1	0.3	0.5	Re 0	1	3
0	0.25	2702.4	132.95	45.478	199.19	112.15	73.229	24.357	33.307	59.794
π/4		2694.8	132.81	45.509	198.04	111.50	72.811	24.368	33.326	59.841
π/2		2679.4	132.181	45.325	196.83	110.81	72.375	24.267	33.193	59.587
0	0.5	181.73	23.125	11.639	1623.6	78.116	31.792	9.7176	8.0928	16.478
π/4		181.378	23.119	11.672	1619.5	77.825	31.661	9.7256	8.1025	16.520
π/2		180.403	23.014	11.651	1610.5	77.360	31.472	9.6825	8.0664	16.485
0	0.75	65.516	7.3505	1.2437	4893.9	359.30	61.779	11.662	5.1984	2.2771
π/4		65.176	7.2964	1.2115	4880.1	357.73	61.451	11.602	5.1571	2.2982
π/2		64.765	7.2323	1.1768	4853.6	355.65	61.102	11.496	5.0963	2.3110

Table 5. Variation of mass flux with $\alpha^*=0.05$ (slip).

t	b	D_a 0.01	0.03	0.05	k_p 0.1	0.3	0.5	Re 0	1	3
0	0.25	0.3573	0.2909	0.3701	0.4070	0.2747	0.2865	0.4171	0.3946	0.3458
π/4		0.3434	0.2947	0.3779	0.4524	0.2966	0.2997	0.4238	0.4020	0.3540
π/2		0.3027	0.2798	0.3721	0.4910	0.3220	0.3145	0.4192	0.3969	0.3472
0	0.5	0.4410	0.4570	0.7866	15.5837	2.0701	1.3008	0.7657	0.7844	0.7756

Table 5.cont. Variation of mass flux with $\alpha^*=0.05$ (slip).

t	b	D_a			k_p			Re		
		0.01	0.03	0.05	0.1	0.3	0.5	0	1	3
$\pi/4$		0.4389	0.4586	0.7893	15.5878	2.0721	1.3024	0.7679	0.7869	0.7786
$\pi/2$		0.4298	0.4550	10.7871	15.5967	2.0758	1.3038	0.7658	0.7848	0.7762
0	0.75	2.2590	0.8163	0.8863	448.2729	11.5510	4.0337	0.8591	0.7759	0.9617
$\pi/4$		2.2589	0.8164	0.8866	448.2731	11.5511	4.0339	10.8592	0.7762	0.9620
$\pi/2$		2.2587	0.8163	0.8859	448.2738	11.5511	4.0336	0.8592	0.7756	0.9614

Table 6. Variation of mass flux with $\alpha^*=0$ (no-slip).

t	b	D_a			k_p			Re		
		0.01	0.03	0.05	0.1	0.3	0.5	0	1	3
0	0.25	0.3367	0.2384	0.2934	0.3278	0.2100	0.2203	0.3352	0.3149	0.2727
$\pi/4$		0.3247	0.2422	0.3012	0.3707	0.2322	0.2335	0.3420	0.3223	0.2807
$\pi/2$		0.2895	0.2280	0.2954	0.4036	0.2555	0.2470	0.3373	0.3171	0.2740
0	0.5	0.4369	0.4068	0.7059	14.7021	1.9076	1.1839	0.6848	0.7042	0.6944
$\pi/4$		0.4350	0.4087	0.7091	14.7061	1.9076	1.1839	0.6874	0.7071	0.6977
$\pi/2$		0.4258	0.4046	10.7064	14.7147	1.9131	1.1865	0.6849	0.7046	0.6948
0	0.75	2.3408	0.8292	0.8339	447.7612	11.6306	4.0438	0.9121	0.7102	0.9181
$\pi/4$		2.3407	0.8293	0.8344	447.7613	11.6307	4.0438	10.9121	0.7102	0.9186
$\pi/2$		2.3404	0.8292	0.8332	447.7616	11.6303	4.0431	0.9121	0.7104	0.9174

The variations in unsteady profiles of velocity, temperature, effects of various shape factor, different nanoparticles influence on velocity and temperature of the liquids are displayed in Figs. 12-16. Figures12 and 13 shows that the unsteady velocity and temperature have an oscillating nature as *t* varies. As the shape factor increases the unsteady temperature profile exhibit oscillating characteristic and the maximum is located at the boundary layer near the suction wall that we can see in Fig.14. We noticed from Fig.15 that various nanoparticles of both regions increase the unsteady velocity oscillates and the maximum at Al_2O_3-Ag when compared with other nanoparticles. Figure16 reveals that, as different nanoparticles of the lower and upper region increase the unsteady temperature oscillates, and the maximum is shifted towards the boundary layer near the suction wall that is at Al_2O_3-Cu for both cases of slip and no-slip conditions when compared with other nanoparticles. Here Al_2O_3-Cu represents that the lower region is occupied by Al_2O_3 and the upper region is filled with Cu with a base fluid having water. Similarly, for Al_2O_3-Ag, Al_2O_3-TiO_2, Al_2O_3-Cu, Cu-TiO_2, Cu-Al_2O_3.

The rate of heat transfer profiles of lower and upper channel walls are displayed in Figs.17-20. Figures 17-20 illustrates the influence of shape factors (brick, cylinder, platelets and sphere) on the Nusselt number of both the walls of the channel. Figures 17 and 20 reveal that Ec increases the lower wall of the channel of Nusselt number decreases and when Rd raises the upper channel wall of heat transfer rate falls. Here we observed that brick-shaped nanoparticles have greater heat transfer rate when compared with other shaped nanoparticles (*sphere<platelets<cylinder<brick*) and we can have noticed from Figs 18 and 19, the rate of heat

transfers of upper walls of the channel raises, when Ec and Rd increases. Here we observed that brick shaped nanoparticle has less heat transfer rate than the other shaped nanoparticles *brick<cylinder<platelets<sphere.*

The flow variables of the velocity of the nanofluid, and temperature of the nanoliquid in Figs. 21-22 with Al_2O_3-water and Cu-water nanofluids with various volume fractions, i.e. $\varphi = 0, 0.03$, and 0.05 in Region-I and Region-II, respectively. When the volume fraction increases in a fluid system, it means that a greater proportion of the total volume is occupied by the fluid particles or components (such as particles, and droplets). When this occurs, the particles come into play which can lead to an increase in velocity. In reality, this phenomenon is also accompanied by a favorable effect caused by the presence of high thermal conductivity, which is smaller than an undesirable effect induced by viscosity that will suppress the flow, with base fluid water, nanofluid cannot flow freely. When the volume fraction rises, the velocity of the nanofluid is higher in the upper region than the lower region it can be seen in Fig.21 due to the rise of solid concentration. The strength of the flow is enhanced by raising φ an increase in the amount of nanoparticles in the fluid and its consequence on the temperature of the fluid and the thermal conductivity of the liquid also improves with a rise in nanoparticles, and energy is transmitted more quickly through the fluid. Consequently, temperature increases as volume fraction increases. This is due to the fact that the flow is accelerated by a high concentration of solid nanoparticles, as seen in Fig.22, which consequently leads to higher energy.

The distributions of the temperature of the liquid and rate of heat transfer under the influence of various shape factors (sphere, brick, cylinder, platelet, column, blade, lamina) are illustrated in Figs.23-25. It is observed that various shape factors raise, the temperature of the liquid increases i.e., (*lamina < blade < column < cylinder < bricks < platelets < sphere*). Increasing the shape factor typically enhances the porous medium's surface area-to-volume ratio. A larger surface area provides for greater contact between the fluid and solid surfaces, which results in more heat transmission. Because of the increased surface area, convective heat transfer takes place, resulting in higher fluid temperatures as seen in Fig.23. It is evident that in Figs 24-25, Nu raises in both walls of the channel as the shape factor value rises, due to the fact that more surface area allows for greater contact between the fluid and solid surfaces, which results in more effective transfer of heat. The increased surface area enhances convective heat transfer, resulting in a greater velocity of heat transfer near the channel walls.

To gain an insight of the characteristics of the flow of different combinations of nanoparticles with, base fluid as water, the distribution of the flow variables are presented in Figs 26-29. From Figs 26 and 27 one can observe that in region-I (Al_2O_3-water) and region-II (Ag -water) has higher velocity and temperature when compared with other nanoparticles i.e. $(Al_2O_3 - Ag > Al_2O_3 - TiO_2 > Cu - Ag > Cu - TiO_2 > Cu - Al_2O_3 > Al_2O_3 - Cu)$ in both slip and no-slip conditions. It is observed from Figs.28 and 29 reveal that $Al_2O_3 - Ag$ has a higher rate of heat transfer in both slip and no-slip conditions i.e., $\left(Al_2O_3 - Ag > Al_2O_3 - TiO_2 > Al_2O_3 - Cu > Cu - Ag > Cu - TiO_2 > Cu - Al_2O_3 \right)$.

To validate the results, a comparative study of the closed-form results is performed in Fig.9 with those obtained by using the shooting technique solved in MATHEMATICA, with a blend of Runge-Kutta 4th-order method. The variation of nanoliquid velocity distribution with the variation of Hartmann number is shown in Fig.30 for the slipcase and the same is illustrated in Fig.31 for the no-slip case. The results are found to be in good agreement.

The shear stress and massflux of both boundaries of the channel with slip $\left(\alpha^* = 0.05 \right)$ and no-slip $\left(\alpha^* = 0 \right)$ conditions, are presented in Tabs 3-6 for the values of different parameter width $\left(b = 0.25, 0.5, 0.75 \right)$ and variation with t. From Tab.3 one can observe that, with the increasing values of Da and k_p the shear stress at the walls decreases. With the rise of Re the shear stress increases at $b = 0.25$, oscillates at $b = 0.5$, and falls at $b = 0.75$. From Tab.4, shear stress decreases, when Da, k_p raises at $b = 0.25 = 0.5 = 0.75$ and stress distribution increases at Re when $b = 0.25 = 0.5$ and oscillates at $b = 0.75$. As, the Da and k_p rise mass flux oscillates and falls with b variation in both regions respectively, whereas R increases mass flux falls at $b = 0.25$ and oscillates at $b = 0.5 = 0.75$ was seen in Tab.5. In Tab.6, when Da raises, oscillations of mass

flux are seen at $b = 0.25$ and 0.75 and increasing of mass flux at $b = 0.5$. As k_p and R raise, mass flux falls at $b = 0.5 = 0.75$ and $b = 0.25$, and a reverse trend can be seen in Da at $b = 0.5$. Oscillations of mass flux can be observed when k_p raises at $b = 0.25$ and Re increases at $b = 0.5$ and $b = 0.75$.

7. Conclusion

The effects of nanoparticles' different shapes on an unsteady pulsating MHD flow of nanofluids through two immiscible fluids in a horizontal channel are discussed. Nanoparticles have generated significant interest due to their unique chemical and physical properties and apply to diverse areas. This model applies to drug delivery systems and also to physiological transport where nanoparticles play an important role. Magnetic forces have been applied to control particle migration, and the energy equation contains radiation's influence. The concluding remarks are as follows:

- The shape factor of the nanoparticle may not have much influence on the velocity distribution.
- The velocity of nanofluid reduces with a rise of nanoparticle volume fraction.
- Temperature of the liquid decreases with an increase of the Darcy number Da. Brick-shaped nanoparticles are higher when compared with cylinder, platelet, and Sphere nanoparticles.
- When Ec, Pr of the upper region, Rd of the lower region raises the rate of heat transfer enhances and when Ec at the lower region and Rd of the upper region enhances the heat transfer rate falls. As Pr increases at the lower region, Nu oscillates.
- The temperature of the liquid increases as the shape factor of the nanoparticles rises. Furthermore, lamina produces higher temperatures in the liquid, when compared with other nanoparticles.
- The rate of heat transfer of lower and upper regions increases, with the shape factor, and for the sphere-shaped nanoparticles, the rate of heat transfer will be higher.

This investigation shows that brick-shaped nanoparticles have the highest rate of heat transfer. The use of cylinder-shaped nanoparticles can be used to control the rise and fall in temperature of the fluid for drug delivery systems. It is essential for industries to control heat transfer through nanofluids, and sphere-shaped nanoparticles can help with it as well.

Nomenclature

B_0	– applied magnetic field
b	– width parameter
$(C_p)_{1f}, (C_p)_{2f}$	– specific heat of capacity at constant pressure in both regions.
H	– frequency parameter
h	– length of the channel
$k = \dfrac{k_{2nf}}{k_{1nf}}$	– ratio of thermal conductivities
k_{1f}, k_{2f}	– thermal conductivity of water
k_{1p}, k_{2p}	– permeability of region-I and II
k_p	– ratio of permeability of the porous medium
M_1, M_2	– Hartmann numbers of both
Nu	– Nusselt number
P	– fluid pressure
Pr	– Prandtl number
q_r	– radiative heat
R_d	– thermal radiation
Re	– Reynolds number
T_{w_1}, T_{w_2}	– temperature of the both the walls regions-I and II
t	– time

u_t	−	unsteady velocity
x, y	−	Cartesian coordinates
α^*	−	velocity slip parameter
α_{nf}	−	ratio of densities of nanoparticles of both regions
β^*	−	temperature slip parameter
β_{nf}	−	ratio of viscosities of region-I and II
γ_{nf}	−	ratio of electrical conductivities of nanoparticles of region-I and II
ε	−	perturbation parameter
θ_1, θ_2	−	fluid temperatures of nanoparticles of both regions.
θ_t	−	unsteady temperature
λ_1	−	non dimensional velocity slip parameter
v_0	−	injection/suction velocity
v_{1f}	−	kinematic viscosity
$\sigma_{1nf}, \sigma_{2nf}$	−	electrical conductivities of region-I and II
τ_1, τ_2	−	shear stress of both regions I and II
ϕ	−	volume fraction of nanoparticle
ω	−	frequency of the pulsating parameter

Appendix

$$p_1 = \frac{A_1}{A_2}, \quad p_2 = \frac{A_5 M_1^2}{A_2} + \frac{1}{Da}, \quad p_3 = -\frac{P_S H^2}{A_2}, \quad p_{4,5} = \frac{R p_1 \pm \sqrt{R^2 p_1^2 + 4 p_2}}{2},$$

$$p_6 = \frac{p_3}{p_2} \quad p_7 = p_2 + \frac{A_1}{A_2} H^2 i, \quad p_8 = -\frac{P_0 H^2}{A_2}, \quad p_{9,10} = \frac{R p_1 \pm \sqrt{R^2 p_1^2 + 4 p_7}}{2}.$$

References

[1] Wang C. and Cheng. P. (1997): *Multiphase flow and heat transfer in porous media.*– Advances in Heat Transfer, vol.30, Elsevier, pp.93-196.

[2] Packham B. and Shall R. (1971): *Stratified laminar flow of two immiscible fluids.*– Mathematical Proceedings of Cambridge Philosophical Society, vol.69, Cambridge University Press, pp.443-448.

[3] Muzumdar A. (1980): *Advances in Transport Process*, vol.1., John Wiley and Sons Ltd.

[4] Bestman A. (1982): *Pulsatile flow in heated porous channel.*– International Journal of Heat and Mass Transfer, vol.25, No.5, pp.675-682.

[5] Bussemer T., Otto. I. and Bodmeier R. (2001): *Pulsatile drug-delivery systems.*– Critical Reviews in Therapeutic Drug Carrier Systems, vol.18, No.5., pp.26.

[6] Zamir M. and Budwig R. (2002): *Physics of pulsatile flow.*– Appl. Mech. Rev., vol.55, No.2, https://doi.org/10.1115/1.1451229.

[7] Chen C., Lin T., Ali. H.M., Amani P. and Yan W.M. (2019): *Bubble dynamics in evaporation flow of r-134a in narrow annular ducts due to flow rate oscillation.*– International Communications in Heat and Mass Transfer, vol.100, pp.27-34.

[8] Mladin E.C. and Zumbrunnen D.A. (2000): *Alterations to coherent flow structures and heat transfer due to pulsations in an impinging air-jet.*– International Journal of Thermal Sciences, vol.39, No.2, pp.236-248.

[9] Radhakrishnamacharya G. and Maiti M. (1977): *Heat transfer to pulsatile flow in a porous channel.*– International Journal of Heat and Mass Transfer, vol.20, No.2, pp.171-173.

[10] Ye Q., Zhang Y. and Wei J. (2021): *A comprehensive review of pulsating flow on heat transfer enhancement.*– Applied Thermal Engineering, vol.196, p.117275.

[11] Kumar P.B. and Suripeddi S. (2021): *A note on the pulsatile flow of hydromagnetic Eyring-Powell nanofluid through a vertical porous channel.*– The European Physical Journal Special Topics, vol.230, pp.1465-1474.

[12] Ezzat M.A. and El-Bary A.A. (2016): *Effects of variable thermal conductivity on Stokes' flow of a thermoelectric fluid with fractional order of heat transfer.*– International Journal of Thermal Sciences, vol.100, pp.305-315.

[13] Choi E.J., Ahn Y. and Do Her Y. (2007): *Size dependence of magnetic properties of co-ferrite nanoparticles.*– Journal of the Korean Physical Society, vol.50, No.2, pp.460-463.

[14] Yoo D.H., Hong K., Hong T., Eastman J. and Yang H.S. (2007): *Thermal conductivity of Al_2O_3/water nanofluids.*– Journal of the Korean Physical Society, vol.51, No.1., pp.84-87., https://doi.org/10.3938/jkps.51.84.

[15] Eastman J.A., Choi U., Li S., Thompson L. and Lee S. (1996): *Enhanced thermal conductivity through the development of nanofluids.*– MRS Online Proceedings Library, vol.457, p.3.

[16] Xie H., Wang J., Xi T., Liu Y., Ai F. and Wu Q. (2002): *Thermal conductivity enhancement of suspensions containing nanosized alumina particles.*– Journal of Applied Physics, vol.91, No.7, pp.4568-4572.

[17] Nield D. and Kuznetsov A., (2009): *The Cheng-Minkowycz problem for natural convective boundary-layer flow in a porous medium saturated by a nanofluid.*– International Journal of Heat and Mass Transfer, vol.52, No.25-26, pp.5792-5795.

[18] Philip J. and Shima P.D. (2012): *Thermal properties of nanofluids.*– Advances in Colloid and Interface Science, vol.183, pp.30-45.

[19] Bachok N., Ishak A. and Pop I. (2012): *Boundary layer flow over a moving surface in a nanofluid with suction or injection.*– Acta Mechanica Sinica, vol.28, pp.34-40.

[20] Kasaeian A., Daneshazarian R., Mahian O., Kolsi L., Chamkha A.J., Wongwises S. and Pop I.(2017): *Nanofluid flow and heat transfer in porous media: a review of the latest developments.*– International Journal of Heat and Mass Transfer, vol.107, pp.778-791.

[21] Khanafer K. and Vafai K. (2019): *Applications of nanofluids in porous medium*: *A critical review.*– Journal of Thermal Analysis and Calorimetry, vol.135, pp.1479-1492.

[22] Vafai K. and Tien C.L., (1981): *Boundary and inertia effects on flow and heat transfer in porous media.*– International Journal of Heat and Mass Transfer, vol.24, No.2, pp.195-203.

[23] Khaled A.R. and Vafai K. (2003): *The role of porous media in modeling flow and heat transfer in biological tissues.*– International Journal of Heat and Mass Transfer, vol.46, No.26, pp.4989-5003.

[24] Cimpean D.S. and Pop I., (2012): *Fully developed mixed convection flow of a nanofluid through an inclined channel filled with a porous medium.*– International Journal of Heat and Mass Transfer, vol.55, No.4, pp.907-914.

[25] Chamkha A.J. and Ismael M.A. (2014): *Natural convection in differentially heated partially porous layered cavities filled with a nanofluid.*– Numerical Heat Transfer, Part A: Applications, vol.65, No.11, pp.1089-1113.

[26] Zhang C., Zheng L., Zhang X. and Chen G. (2015): *Mhd flow and radiation heat transfer of nanofluids in porous media with variable surface heat flux and chemical reaction.*– Applied Mathematical Modelling, vol.39, No.1, pp.165-181.

[27] Vijayalakshmi A. and Srinivas S., (2017): *A study on the hydromagnetic pulsating flow of a nanofluid in a a porous channel with thermal radiation.*– Journal of Mechanics, vol.33, No.2, pp.213-224.

[28] Umavathi J. and Hemavathi K. (2019): *Flow and heat transfer of composite porous medium saturated with nanofluid.*– Propulsion and Power Research, vol.8, No.2, pp.173-181.

[29] Nazeer M., Ali N., Ahmad F. and Latif M. (2020): *Numerical and perturbation solutions of third-grade fluid in a porous channel: boundary and thermal slip effects.*– Pramana, vol.94, pp.1-15.

[30] Ezzat M.A., El-Bary A.A. and Morsey M.M. (2010): *Space approach to the hydro-magnetic flow of a dusty fluid through a porous medium.*– Computers & Mathematics with Applications*, vol.59, No.8, pp.2868-2879.

[31] Daniel Y.S., Aziz Z.A., Ismail Z. and Salah F. (2017): *Effects of thermal radiation, viscous and Joule heating on electrical MHD nanofluid with double stratification.*– Chinese Journal of Physics, vol.55, No.3, pp.630-651.

[32] Govindarajulu K. and Subramanyam Reddy A. (2022): *Magnetohydrodynamic pulsatile flow of third-grade hybrid nanofluid in a porous channel with Ohmic heating and thermal radiation effects.*– Physics of Fluids, vol.34, No.1, p.013105.

[33] Wahid N.S., Arifin N.M., Pop I., Bachok N. and Hafidzuddin M.E.H. (2022): *MHD stagnation-point flow of nanofluid due to a shrinking sheet with melting, viscous dissipation, and Joule heating.*– Alexandria Engineering Engineering Journal, vol.61, No.12, pp.12661-12672.

[34] Hayat T., Sajjad R., Abbas Z., Sajid M. and Hendi A.A. (2011): *Radiation effects on MHD flow of Maxwell fluid in a channel with porous medium.*– International Journal of Heat and Mass Transfer, vol.54, No.4, pp.584-862.

[35] Hatami M., Nouri R. and Ganji D., (2013): *Forced convection analysis for MHD Al_2O_3-water nanofluid flow over a horizontal plate.*– Journal of Molecular Liquids, vol.187, pp.294-301.

[36] Sheikholeslami M., Ganji D.D., Javed M.Y. and Ellahi R. (2015): *Effect of thermal radiation on magnetohydrodynamics nanofluid flow and heat transfer by means of a two-phase model.*– Journal of Magnetism and Magnetic Materials, vol.374, pp.36-43.

[37] Sandeep N. and Reddy M.G. (2017): *Heat transfer of nonlinear radiative magnetohydrodynamic Cu-water nanofluid flow over two different geom*etries.– Journal of Molecular Liquids, vol.225, pp.87-94.

[38] Ezzat M., El-Bary A.A. and Ezzat S. (2011): *Combined heat and mass transfer for unsteady MHD flow of perfect conducting micropolar fluid with thermal relaxation.*– Energy Conversion and Management, vol.52, No.2, pp.934-945.

[39] Raisi A., Ghasemi B. and Aminossadati S. (2011): *A numerical study on the forced convection of laminar nanofluid in a microchannel with both slip and no-slip conditions.*– Numerical Heat Transfer, Part A: Applications, vol.59, No.2, pp.114-129.

[40] Bitla P. and Iyengar T., (2013): *Effects of slip on the pulsating flow of an incompressible micropolar fluid through a porous medium between two parallel plates.*– Journal of Porous Media, vol.16, No.8., pp.769-775., DOI:10.1615/JPorMedia.v16.i8.70.

[41] Adesanya S.O. and Makinde O.D. (2014): *MHD oscillatory slip flow and heat transfer in a channel filled with porous media.*– UPB Sci. Bull. Series A, vol.76, pp.197-204.

[42] Srinivas S., Vijayalakshmi A., Reddy A.S. and Ramamohan T. (2016): *MHD flow of a nanofluid in an expanding or contracting porous pipe with chemical reaction and heat source/sink.*– Propulsion and Power Research, vol.5, No.2, pp.134-148.

[43] Vijayalakshmi A. and Srinivas S. (2016): *Asymmetric flow of a nanofluid between expanding or contracting permeable walls with thermal radiation.*– Frontiers in Heat and Mass Transfer, vol.7, No.10, pp.1-11.

[44] Sucharitha G., Lakshminarayana P. and Sandeep N. (2017): *Joule heating and wall flexibility effects on the peristaltic flow of magnetohydrodynamic nanofluid.*– International Journal of Mechanical Sciences, vol.131, pp.52-62.

[45] Goodarzi M., Javid S., Sajadifar A., Nojoomizadeh M., Motaharipour S.H., Bach Q.V. and Karimipour A. (2018): *Slip velocity and temperature jump of a non-newtonian nanofluid, aqueous solution of carboxymethyl cellulose/aluminum oxide nanoparticles, through a microtube.*– International Journal of Numerical Methods for Heat & Fluid Flow, vol.29, No.5, pp.1606-1628.

[46] Qi W., Wang M. and Su Y. (2002): *Size effect on the lattice parameters of nanoparticles.*– Journal of Materials Science Letters, vol.21, pp.877-878.

[47] Qi W., Wang M. and Xu G. (2003): *Erratum to the particle size dependence of cohesive energy of metallic nanoparticles.*– Chemical Physics Letters, vol.3, No.376, p.538.

[48] Nanda K., Sahu S., and Behera S. (2002): *Liquid-drop model for the size-dependent melting of low-dimensional systems.*– Physical review A, vol.66, No.1, p.013208.

[49] Chamkha A.J., Dogonchi A. and Ganji D. (2018): *Magnetohydrodynamic nanofluid natural convection in a cavity under thermal radiation and shape factor of nanoparticles impacts: a numerical study using cvfem.*– Applied Sciences, vol.8, No.12, p.2396.

[50] Sobamowo G. (2019): *Free convection flow and heat transfer of nanofluids of different shapes of nano- sized particles over a vertical plate at low and high Prandtl numbers.*– Journal of Applied and Computational Mechanics, vol.5, No.1, pp.13-39.

[51] Shah Z., Babazadeh H., Kumam P., Shafee A. and Thounthong P. (2019): *Numerical simulation of magnetohydrodynamic nanofluids under the influence of shape factor and thermal transport in a porous media using cvfem.*– Frontiers in Physics, vol.7, p.164.

[52] Dogonchi A.S., Armaghani T., Chamkha A.J. and Ganji D. (2019): *Natural convection analysis in a cavity with an inclined elliptical heater subject to shape factor of nanoparticles and magnetic field.*– Arabian Journal for Science and Engineering, vol.44, pp.7919-7931.

[53] Cele T. (2020): *Preparation of Nanoparticles.*– Engineered Nanomaterials-Health and Safety.

[54] Hazarika S., Ahmed S. and Chamkha A.J. (2021): *Investigation of nanoparticles Cu, Ag, Fe_3O_4 on thermophoresis and viscous dissipation of MHD nanofluid over a stretching sheet in a porous regime: a numerical modeling.*– Mathematics and Computers in Simulation, vol.182, pp.819-837.

[55] Ananth Subray P., Hanumagowda B., Varma S. and Hatami M. (2022): *The impacts of shape factor and heat transfer on the two-phase flow of nano and hybrid nanofluid in a saturated porous medium.*– Scientific Reports, vol.12, No.1, p.21864.

[56] Saranya S. and Al-Mdallal Q.M., (2021): *Computational study on nanoparticle shape effects of Al_2O_3-slicon oil nanofluid flow over a radially stretching rotating disk.*– Case Studies in Thermal Engineering, vol.25, p.100943.

[57] Zubair T., Usman M., Nisar K.S., Hamid M., Mahmoud E.E. and Yahia I. (2022): *Investigation of shape effects of Cu-nanoparticle on heat transfer of MHD rotating flow over a nonlinear stretching sheet.*– Alexandria Engineering Journal, vol.61, No.6, pp.4457-4466.

[58] Akbar A.A., Ahammad N.A., Awan A.U., Hussein A.K., Gamaoun F., Tag-Eldin E.M. and Ali B. (2022): *Insight into the role of nanoparticle shape factors and diameter on the dynamics of rotating water-based fluid.*– Nanomaterials, vol.12, No.16, p.2801.

[59] Chamkha A.J., Umavathi J.C. and Mateen A., (2004): *Oscillatory flow and heat transfer in two immiscible fluids.*– International Journal of Fluid Mechanics Research, vol.31, No.1., pp.24, DOI: 10.1615/InterJFluidMechRes.v31.i1.20.

[60] Umavathi J., MatPrandtl Chamkha A.J. and Al-Mudhaf A. (2006): *Oscillatory Hartmann two-fluid flow and heat transfer in a horizontal channel.*– International Journal of Applied Mechanics and Engineering, vol.11, No.1, pp.155-178.

[61] Padma Devi M. and Srinivas S. (2022): *Thermal characteristics on two immiscible fluid flow in a porous space with a time-dependent pressure gradient.*– Proceedings of the Institution of Mechanical Engineers, Part E: Journal of Process Mechanical Engineering, vol.236, No.6, pp.2480-2490.

[62] Devi M.P. and Srinivas S. (2023): *Two layered immiscible flow of viscoelastic liquid in a vertical porous channel with hall current, thermal radiation, and chemical reaction.*– International Communications in Heat and Mass Transfer, vol.142, p.106612.

[63] Hamilton R.L. and Crosser O. (1962): *Thermal conductivity of heterogeneous two-component systems.*– Industrial & Engineering Chemistry Fundamentals, vol.1, No.3, pp.187-191.